Lattice dynamics simulation of Cs_2CdBr_4 crystal

1999 J. Phys.: Condens. Matter 11 3615

(http://iopscience.iop.org/0953-8984/11/17/319)

J. Phys.: Condens. Matter **11** (1999) 3615–3628. Printed in the UK PII: S0953-8984(99)01521-0

Lattice dynamics simulation of Cs_2CdBr_4 crystal

Ya Shchur†‡, S Kamba‡ and J Petzelt‡

† Institute of Physical Optics, Dragomanova 23, Lviv, UA-290005, Ukraine
‡ Institute of Physics, Academy of Sciences of the Czech Republic, Na Slovance 2, 18221 Prague 8, Czech Republic

Received 2 February 1999

Abstract. Lattice dynamics calculations for the Cs_2CdBr_4 crystal in the high-temperature orthorhombic phase ($Pnma$) and in the monoclinic phase ($P2_1/n11$) at ∼195 K were carried out. The model was based on the atom–atom potential function which comprised the long-range Coulombic, short-range and covalent interactions. Comparison of the calculated phonon frequencies with the experimental ones obtained from far-infrared reflectivity and Raman scattering measurements gives a reasonable agreement in most cases. A possible origin of the incommensurate phase transition was discussed on the basis of a coupling between low-lying Σ_2 phonon branches. Using group-theory analysis and the calculated phonon dispersion branches, it is shown that the $P2_1/n11$–$P\bar{1}$ phase transition is very probably induced by the condensation of a phonon mode at the Brillouin zone boundary.

1. Introduction

In the previous paper [1] (hereafter denoted as paper I) we have reported on a detailed far-infrared (FIR) investigation of Cs_2CdBr_4 crystal in all of its structural phases. Our main attention was attracted to the temperature evolution of the lattice vibrations in Cs_2CdBr_4 at the phase transitions, in particular at the incommensurate phase transition. Experimental FIR reflectivity spectra were evaluated on the basis of a phenomenological four-parameter oscillator model [2]. It would be of interest to understand some lattice dynamics peculiarities of Cs_2CdBr_4 crystal on a more microscopic level. For example, it is desirable to obtain information about the nature of modes observed experimentally, to perform their eigenvector assignment, to explain the origin of the TO–LO mode splitting and to try to understand the phase transitions.

The first theoretical work on the microscopic basis for the lattice dynamics study of A_2BX_4 compounds was done by Haque and Hardy [3]. As was shown in their paper, in the framework of the rigid-ion model for K_2SeO_4 crystal, the lowest-lying Σ_2 branch has a minimum near $\boldsymbol{k} = (1/3)\boldsymbol{a}^*$, in agreement with the neutron scattering results [4]. A semi-empirical version of the rigid-ion model was used also for the study of the temperature changes of the calculated phonon dispersion relation for K_2SeO_4 [5]. Softening of the Σ_2 branch was found for this model at $\boldsymbol{k} = 0.27\boldsymbol{a}^*$. A very careful lattice dynamics study of $LiKSO_4$ crystal in the two phases (space groups $P6_3$ and $P31c$) was carried out by Chaplot *et al* [6]. Taking into account the Coulombic and short-range interactions, as well as covalent interactions within SO_4 groups, the authors of reference [6] have shown that softening of the E_1^+ symmetry branch occurred at a point near to $0.4\boldsymbol{c}^*$. Phonon dispersion curves were calculated also for the $CsLiSO_4$ crystal [7] for both $Pnma$ and $P112_1/n$ structures. However, in the $Pnma$ phase

0953-8984/99/173615+14$19.50

two unstable branches represented by imaginary frequencies appeared, which implies that the $Pnma$ structure of $CsLiSO_4$ crystal is unstable. Recently, a lattice dynamics calculation for the Cs_2HgCl_4 crystal in the framework of the rigid-ion model was carried out to interpret Raman scattering measurements in the $Pnma$ phase [8].

Another simulation of the lattice dynamics was performed using *ab initio* potentials [9–11]. By means of molecular dynamics and lattice dynamics calculations, it was shown that the instability appears at the point $\boldsymbol{k} = (1/2)(\boldsymbol{b}^* + \boldsymbol{c}^*)$ in the $Pna2_1$ phase of Rb_2ZnCl_4 [10] and K_2ZnCl_4 [11] crystals. This type of instability leads to phase transitions which are accompanied by unit-cell doubling along both the ***b***- and the ***c***-axis.

In this paper we report on the results of the lattice dynamics simulation of Cs_2CdBr_4 in the high-temperature phase I ($Pnma$) and monoclinic phase IV ($P2_1/n11$) (see the sequence of phase transitions in paper I).

2. Crystal structure and group-theory classification of lattice vibrations

At room temperature the four molecules of Cs_2CdBr_4 are arranged in the orthorhombic $Pnma$ unit cell ($a = 10.235$ Å, $b = 7.946$ Å, $c = 13.977$ Å [12]) as shown in figure 1. The atomic coordinates at room temperature (phase I) [12] and at 195 K (phase IV, space group $P2_1/n11$, $a = 10.201$ Å, $b = 7.856$ Å, $c = 13.949$ Å, $\alpha = \beta = \gamma = 90^\circ$ [13]) are listed together with the corresponding distances within the tetrahedra in table 1. At the phase transition into

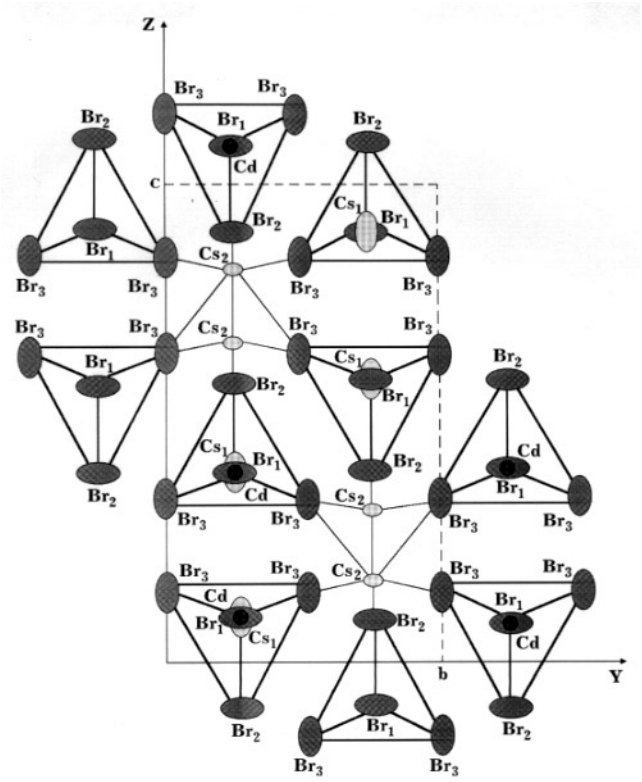

Figure 1. Cs_2CdBr_4 crystal structure (according to reference [12]).

Table 1. Atomic coordinates of Cs_2CdBr_4 crystal and distances within a tetrahedron in the *Pnma* (I) phase at room temperature (according to reference [12]) and in the $P2_1/n11$ phase (IV) taken at 195 K (according to reference [13]).

Pnma				$P2_1/n11$			
	x	*y*	*z*		*x*	*y*	*z*
Cs1	0.1236	0.25	0.0960	Cs1	0.1224	0.2596	0.0997
Cs2	−0.0170	0.25	0.6762	Cs2	−0.0158	0.2595	0.6756
Cd	0.2225	0.25	0.4236	Cd	0.2226	0.2472	0.4243
Br1	−0.0243	0.25	0.4119	Br1	−0.0264	0.2532	0.4140
Br2	0.3204	0.25	0.5926	Br2	0.3228	0.2875	0.5917
Br3	0.3209	−0.0094	0.3426	Br3	0.3237	−0.0312	0.3623
				Br4	0.3131	0.4844	03176
Cd–Br1	2.532 Å			Cd–Br1	2.532 Å		
Cd–Br2	2.566 Å			Cd–Br2	2.572 Å		
Cd–Br3	2.558 Å			Cd–Br3	2.587 Å		
				Cd–Br4	2.572 Å		

the monoclinic $P2_1/n11$ phase III or IV (the authors of reference [13] supposed that in the temperature region $237 > T > 158$ K there exists only one phase instead of two (phases III and IV)), the mirror (m) and the $\boldsymbol{a}$-glide planes vanish due to the rotation of $CdBr_4^{2-}$ tetrahedra by 7–8° about the $\boldsymbol{a}$-axis. At the same time, the tetrahedra become more distorted. Thus the difference between the maximum and minimum of Cd–Br distances increases from 0.034 Å at room temperature to 0.055 Å at 195 K.

As mentioned in paper I, internal vibrations of $CdBr_4^{2-}$ groups have extremely low frequencies ($\nu_2 = 49$, $\nu_4 = 61$ or 75, $\nu_1 = 161$ and $\nu_3 = 177$ cm^{-1} [14]), which are located in the region usual for external vibrations. Owing to this, the rigid-ion approximation is not justified for the lattice dynamics study and instead we have used an atomic model [15] which makes no distinction between the external and internal vibrations.

The classification of 84 normal modes in the initial phase I according to the irreducible representations for the Brillouin zone centre (the Γ point), boundary points (X, Y, Z points) [16] and for the main directions (Σ, Δ, Λ) in the Brillouin zone was performed in paper I where it is given as table 3.

Using the standard group-theoretical analysis [15] we have obtained the form of the symmetry coordinates for the Γ, X, Y, Z, Σ, Δ and Λ wave vectors which correspond to the atomic displacements classified according to the irreducible representations. According to

Table 2. Compatibility relations between the irreducible representations along the main directions of the Brillouin zone in the $P2_1/n11$ (C_{2h}^5) phase ($0 < \mu_1, \mu_2, \mu_3 < 1/2$).

Γ ($\boldsymbol{k}=\boldsymbol{0}$)	Σ ($\boldsymbol{k}=\mu\boldsymbol{a}^*$)	X ($\boldsymbol{k}=\frac{1}{2}\boldsymbol{a}^*$)	Γ ($\boldsymbol{k}=\boldsymbol{0}$)	Δ ($\boldsymbol{k}=\mu\boldsymbol{b}^*$)	Y ($\boldsymbol{k}=\frac{1}{2}\boldsymbol{b}^*$)	Γ ($\boldsymbol{k}=\boldsymbol{0}$)	Λ ($\boldsymbol{k}=\mu\boldsymbol{c}^*$)	Z ($\boldsymbol{k}=\frac{1}{2}\boldsymbol{c}^*$)
$21A_g$			$21A_g$			$21A_g$		$21Z_1$
	$42\Sigma_1$			$42\Delta_1$			$42\Lambda_1$	
$21A_u$			$21B_u$			$21B_u$		$21Z_4$
		84X			84Y			
$21B_g$			$21B_g$			$21B_g$		$21Z_3$
	$42\Sigma_2$			$42\Delta_2$			$42\Lambda_4$	
$21B_u$			$21A_u$			$21A_u$		$21Z_2$

Table 3. Comparison of the calculated and experimental values of the phonon frequencies (in cm^{-1}) near the Brillouin zone centre at room temperature in the *Pnma* phase (QTO: quasi-transverse optic modes; QLO: quasi-longitudinal optic modes—see the text). ν_1 and ν_3 are symmetric and asymmetric internal stretching vibrations of $CdBr_4^{2-}$ groups, respectively. Our experimental Raman data are compared with the data from reference [20].

$A_g(xx, yy, zz)$			$B_{1g}(xy)$			$B_{2g}(xz)$			$B_{3g}(yz)$		
Calc-	Raman		Calc-	Raman		Calc-	Raman		Calc-	Raman	
ulations	Our data	[20]	ulations	Our data	[20]	ulations	Our data	[20]	ulations	Our data	[20]
23	21	18	23	21		26	22		23	22	
27	28	28	28	39	39	30			33		28
31			46	43	43	33			40	43	46
36			68	66	66	50			64		
44	42	40	70		71	54	52	54	68	68	71
54		58	105		81	57			ν_1 107		
69	69	70	145	174	176	73	65	68	ν_3 146	172	175
93	81	84	ν_3 181	183	183	93		81	ν_3 181	181	183
135						137					
143						146					
ν_1 175	173	175				ν_1 177	172	175			
ν_3 187		184				ν_3 188	187	186			
ν_3 206	194	200				ν_3 206		198			

table 5 of paper I, the normal modes in the phase IV (and III) at the Brillouin zone centre are classified as follows:

$$\Gamma(\mathrm{IV}) = 21A_g + 21B_g + 21A_u + 21B_u.$$

The correlation diagram for the irreducible representation in phase IV is presented in table 2.

3. Model

It is obvious that Cs, Cd and Br atoms in the Cs_2CdBr_4 crystal are linked by different types of bond. For simulation of ionic bonds between Cd and Br atoms which belong to different $CdBr_4^{2-}$ groups and Cs atoms, we have used a two-body interatomic potential in the following form [17]:

$$V(r_{kk'}) = \frac{e^2}{4\pi\varepsilon_0}\frac{Z(k)Z(k')}{r_{kk'}} + a\exp\left(-\frac{br_{kk'}}{R(k)+R(k')}\right) \tag{1}$$

where the first term corresponds to the long-range Coulombic interactions and the second one describes the short-range repulsive interaction of Born–Mayer type. ε_0 is the static permittivity; $Z(k)$ and $R(k)$ are the effective charge and radius of atom k, respectively; $r_{kk'}$ is the distance between the atoms k and k'.

In order to approximate the covalent stretching interactions within the Cd–Br bond, we have used, in accordance with [6], the following expression:

$$V(r_{\mathrm{CdBr}}) = -D\exp\left(-\frac{n}{2}\frac{(r_{\mathrm{CdBr}}-r_0)^2}{r_{\mathrm{CdBr}}}\right) \tag{2}$$

where r_{CdBr} is the distance between covalently linked Cd and Br atoms; n, D and r_0 are treated as parameters.

Table 3. (Continued)

A_u	B_{1u}			B_{2u}			B_{3u}		
Calculations	IR [1]	Calculations		IR [1]	Calculations		IR [1]	Calculations	
		Acoustic			Acoustic			Acoustic	
16		17	QTO, k_x	34	30	TO		24	QLO, k_x
30			TO, k_y	37	38	LO		24	TO, k_y
36		18	QLO, k_z	47	42	TO			QTO, k_z
65	31	28	QTO, k_x	57	60	LO	33	33	QLO, k_x
72			TO, k_y	61	64	TO	32	32	TO, k_y
103	34	34	QLO, k_z	62	65	LO			QTO, k_z
142	44	44	QTO, k_x	70	70	TO	44	47	QLO, k_x
ν_3 180			TO, k_y	81	73	LO	43	43	TO, k_y
	50	49	QLO, k_z		103	TO			QTO, k_z
	58	50	QTO, k_x		103	LO	51	51	QLO, k_x
			TO, k_y		143	TO	49	49	TO, k_y
	61	61	QLO, k_z		146	LO			QTO, k_z
	64	62	QTO, k_x	ν_3 183	181	TO	69	69	QLO, k_x
			TO, k_y	196	187	LO	65	52	TO, k_y
	69	66	QLO, k_z						QTO, k_z
	71	71	QTO, k_x				79	73	QLO, k_x
			TO, k_y				75	73	TO, k_y
	84	72	QLO, k_z						QTO, k_z
			QTO, k_x				96	93	QLO, k_x
		98	TO, k_y				85	93	TO, k_y
			QLO, k_z						QTO, k_z
			QTO, k_x					138	QLO, k_x
		135	TO, k_y					135	TO, k_y
		136	QLO, k_z						QTO, k_z
		142	QTO, k_x					142	QLO, k_x
			TO, k_y					141	TO, k_y
		144	QLO, k_z						QTO, k_z
	ν_1 173	176	QTO, k_x				ν_1	182	QLO, k_x
			TO, k_y					181	TO, k_y
	174	182	QLO, k_z						QTO, k_z
	ν_3 184	187	QTO, k_x				ν_3 197	193	QLO, k_x
			TO, k_y				191	187	TO, k_y
	196	188	QLO, k_z						QTO, k_z
			QTO, k_x				ν_3 205	205	QLO, k_x
	ν_3 199	205	TO, k_y				198	204	TO, k_y
	201		QLO, k_z						QTO, k_z

For the simulation of bending vibrations which are determined by the Br–Br interactions within the same $CdBr_4^{2-}$ group, the following potential was used [6]:

$$V(r_{\mathrm{BrBr}}) = \frac{e^2}{4\pi\varepsilon_0}\frac{Z^2(\mathrm{Br})}{r_{\mathrm{BrBr}}} + Sa\exp\left(-\frac{br_{\mathrm{BrBr}}}{2R(\mathrm{Br})}\right) - \frac{W}{r_{\mathrm{BrBr}}^6} \tag{3}$$

where S and W are parameters. The first and second terms in (3) have meanings similar to those used in expression (1) and the third one is the potential of the van der Waals type.

The unknown parameters in expression (1) were determined from the lattice equilibrium conditions [18] and from the condition of electroneutrality of the whole Cs_2CdBr_4 molecule. The a- and b-constants have the values $a = 1822$ eV and $b = 12.364$.

The parameters of the bond-stretching (equation (2)) and Br–Cd–Br angle-bending (equation (3)) potentials were obtained from the condition of agreement between the calculated and experimental frequencies of IR- and Raman-active modes. The experimental IR mode frequencies were taken from paper I. The Raman mode frequencies were taken from our own unpublished room temperature measurements which are as regards the main features in agreement with the previous Raman studies of Cs_2CdBr_4 [19, 20] (see table 3).

4. Results and discussion

As follows from structural considerations (see table 1), it is reasonable to assume different values of the charges $Z(k)$ and radii $R(k)$ for (i) Cs1 and Cs2 and (ii) Br1, Br2 and Br3 atoms. As was shown in reference [13], there are eleven Br ligand atoms around Cs1 and nine Br atoms around Cs2, which leads to much a smaller valence of Cs1 compared to Cs2. The calculated valence sum in the $Pnma$ phase around Cs1 was 0.53 whereas that around Cs2 was 1.02. In the $P2_1/n11$ phase the valence of the Cs1 atom increases to 0.63 while that of Cs2 remains at 1.01 [13]. Our calculations based on the conditions for crystal structure stability (i.e. minimization of the resulting forces acting on individual atoms) yield the values presented in table 4. As one can see, the charge values of Cs1 and Cs2 atoms obtained are in a very good agreement with those proposed in reference [13]. Suitable values of the rest of the parameters, namely $D = 2.807$ eV, $r_0 = 2.208$ Å, $n = 7.372$ Å^{-1}, $S = 1358$ and $w = 1008$ eV Å^6, were used for the calculations for both $Pnma$ and $P2_1/n11$ phases.

Table 4. Effective charges and radii used in the atomic model simulation of Cs_2CdBr_4 crystal in the $Pnma$ and $P2_1/n11$ phases.

$Pnma$							
Type of ion, k	Cs1	Cs2	Cd	Br1	Br2	Br3	
$Z(k)$	0.533	1.099	0.727	−0.566	−0.643	−0.575	
$R(k)$	2.853	2.808	0.833	1.506	1.524	1.546	
$P2_1/n11$							
Type of ion, k	Cs1	Cs2	Cd	Br1	Br2	Br3	Br4
$Z(k)$	0.64	1.04	0.642	−0.549	−0.69	−0.543	−0.540
$R(k)$	2.900	2.723	0.950	1.461	1.414	1.580	1.570

Using the above-specified model parameters (table 4) and the crystal structure (table 1), we have calculated the phonon dispersion relations for the $Pnma$ (I) and $P2_1/n11$ (IV) phases. The lattice dynamics simulation of Cs_2CdBr_4 crystal was carried out by means of the program DISPR [21] modified by us in such a way as to take into account the stretching and bending interactions within the $CdBr_4^{2-}$ groups.

4.1. Phase I (Pnma)

A comparison of the phonon frequencies calculated near the Brillouin zone centre along the main directions of the Brillouin zone at the points $\boldsymbol{k}_{a^*}, \boldsymbol{k}_{b^*}, \boldsymbol{k}_{c^*} \simeq 0.001$ with those obtained from IR and Raman measurements is given in table 3. In the case of the IR-active B_{1u} and B_{3u} modes, it is not always the case that all atomic displacements in the eigenvectors are directed along the dipole moment direction of the corresponding eigenvectors. That is, from the analysis of corresponding symmetry coordinates and eigenvectors it follows that the displacements for

both B_{1u} and B_{3u} symmetry types are localized generally in the xz-plane, whereas their dipole moments are directed along the z-axis and x-axis, respectively, as required by symmetry (see tables 2 and 4 in paper I). We call these modes quasi-transverse optical (QTO) and quasi-longitudinal optical (QLO) depending on whether the dipole moment is perpendicular to or along the propagation vector direction. As one can see from table 3, there is a reasonable agreement between theory and experiment for most TO and QTO modes. A slightly less good agreement was found for LO and QLO modes.

Table 5. The correlation diagram of the internal modes of Cs_2CdBr_4 in the high-temperature ($Pnma$) phase (according to reference [20]).

Free-ion $(CdBr_4)^{2-}$ symmetry T_d	Site symmetry C_{1h}	Factor-group symmetry C_{2h}
		$6A_g(\nu_1, \nu_2, 2\nu_3, 2\nu_4)$
$A_1(\nu_1)$	$6A'(\nu_1, \nu_2, 2\nu_3, 2\nu_4)$	$6B_{2g}(\nu_1, \nu_2, 2\nu_3, 2\nu_4)$
		$6B_{1u}(\nu_1, \nu_2, 2\nu_3, 2\nu_4)$
$E(\nu_2)$		$6B_{3u}(\nu_1, \nu_2, 2\nu_3, 2\nu_4)$
		$3B_{1g}(\nu_2, \nu_3, \nu_4)$
$2F_2(\nu_3, \nu_4)$	$3A''(\nu_2, \nu_3, \nu_4)$	$3B_{3g}(\nu_2, \nu_3, \nu_4)$
		$3A_u(\nu_2, \nu_3, \nu_4)$
		$3B_{2u}(\nu_2, \nu_3, \nu_4)$

It should be stressed that in the case of Cs_2CdBr_4 crystal, division of the normal modes into the external and internal ones is not possible. Using the eigenvector analysis, one can see that all of the phonon modes have both external and internal components. However, the last three highest-frequency modes of A_g, B_{2g}, B_{1u} and B_{3u} symmetry and also one of the highest-frequency modes of B_{1g}, B_{3g}, A_u and B_{2u} types have predominantly internal character. The relevant assignment of these internal stretching ν_1- and ν_3-vibrations is indicated in table 3. This is in good agreement with the correlation diagram of internal vibrations of $CdBr_4^{2-}$ groups (see table 5). Nevertheless, according to the eigenvector analysis the second- and third-highest-frequency modes of B_{1g} (at 105 and 145 cm^{-1}), B_{3g} (at 107 and 146 cm^{-1}), A_u (at 103 and 142 cm^{-1}) and B_{2u} (at 103 and 143 cm^{-1}) symmetry also reveal predominantly internal type (e.g. the displacements of Cd and Br atoms in the B_{2u} modes above 140 cm^{-1} are three to four orders of magnitude larger than those in the other B_{2u} modes). It is worth noting that the second highest observed B_{1g} and B_{3g} modes (at 174 and 172 cm^{-1}, respectively) have appreciably higher frequency than calculated. This indicates that the internal (ν_3) character is even stronger than that calculated in our model.

The calculated phonon dispersion relations along the main $\boldsymbol{a}^*$-, $\boldsymbol{b}^*$- and $\boldsymbol{c}^*$-directions of the Brillouin zone in the $Pnma$ phase are presented in figure 2. As can be seen from this figure, the phonon modes become twofold degenerate at the X, Y and Z points of the Brillouin zone boundary, as follows from symmetry considerations (see table 3 in paper I).

It is worth drawing attention to the peculiarity of the low-frequency part of the dispersion branches along the $\boldsymbol{a}^*$-direction shown in figure 3. As one can see, the phenomenon of anticrossing of the two lowest TO branches of Σ_2 symmetry seems to occur due to the repulsion of these branches. In reference [22] it was proposed that the mechanism of the I $\rightarrow$ II phase transition consists in just such a coupling of two low-lying Σ_2 branches. A coupling term like $S_{\boldsymbol{k}_i} R^*_{\boldsymbol{k}_i} - S^*_{\boldsymbol{k}_i} R_{\boldsymbol{k}_i}$ (where $S_{\boldsymbol{k}=\boldsymbol{0}}$ and $R_{\boldsymbol{k}=\boldsymbol{0}}$ are the corresponding normal-mode coordinates at the Γ point) in the free-energy expansion is equivalent to a Lifshitz-like invariant in the

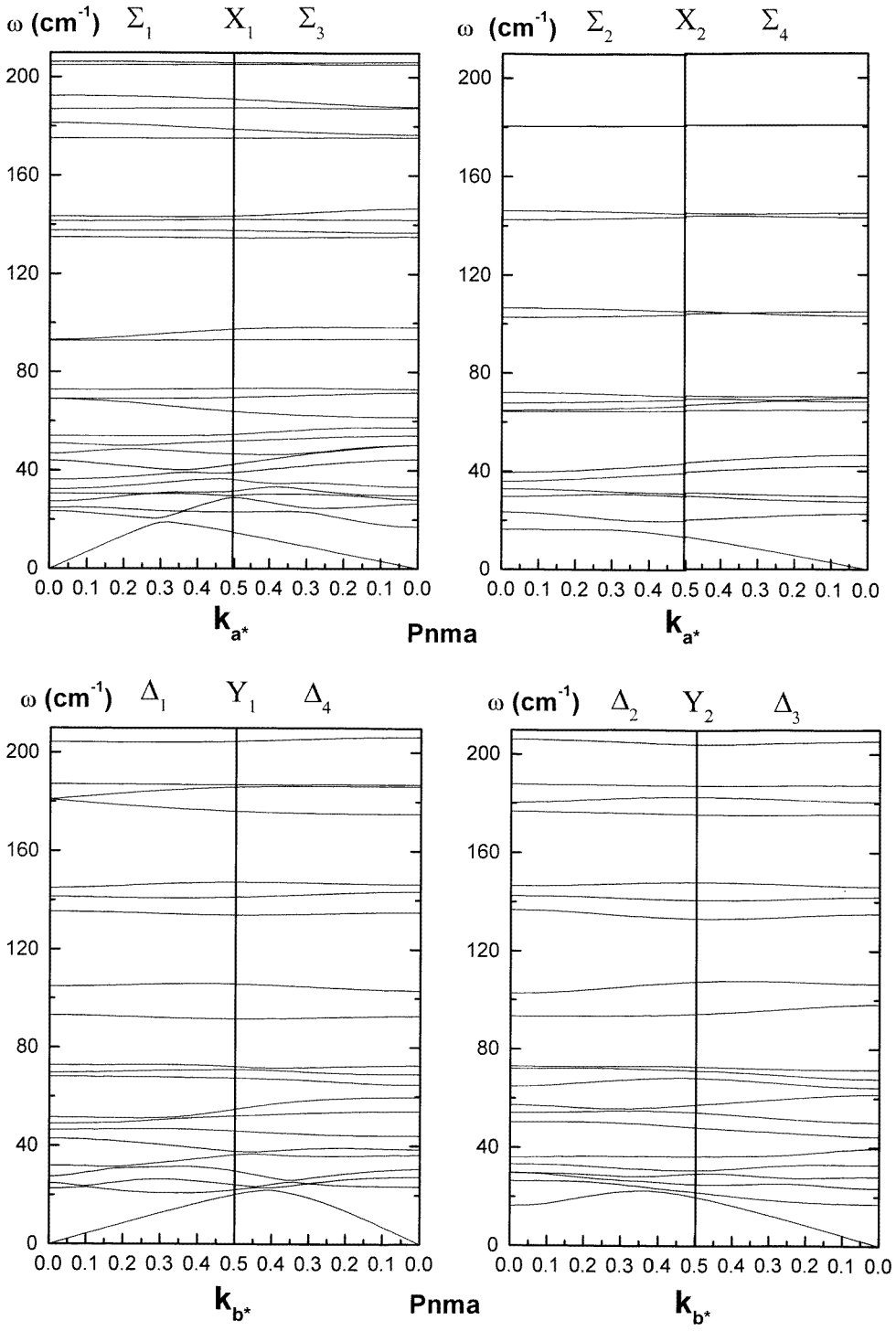

Figure 2. Phonon dispersion curves of Cs_2CdBr_4 in the *Pnma* phase. The figures are drawn in the extended-zone scheme.

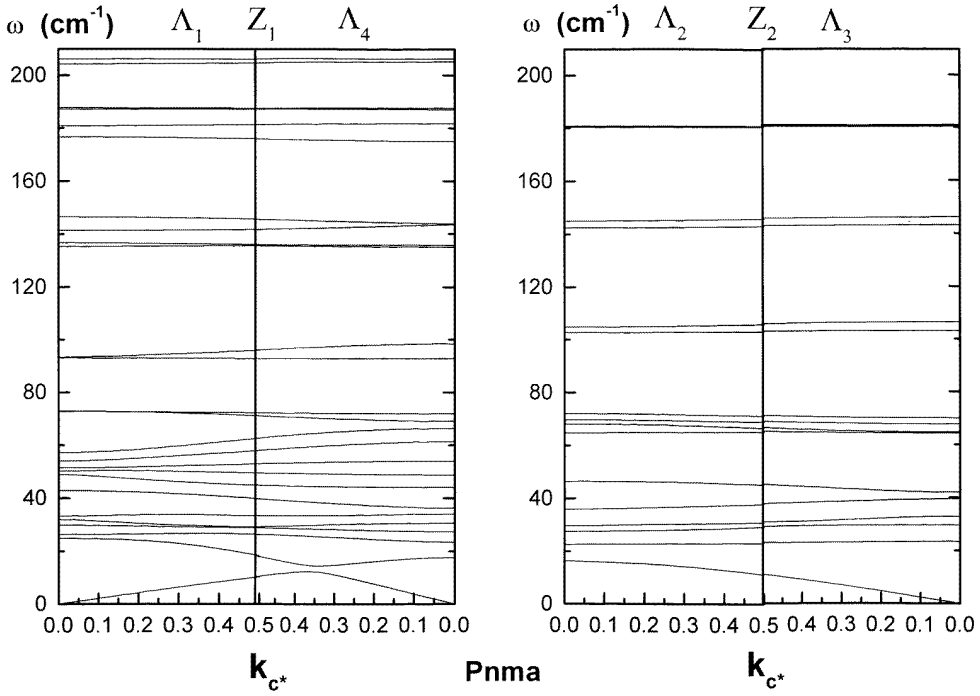

Figure 2. (Continued)

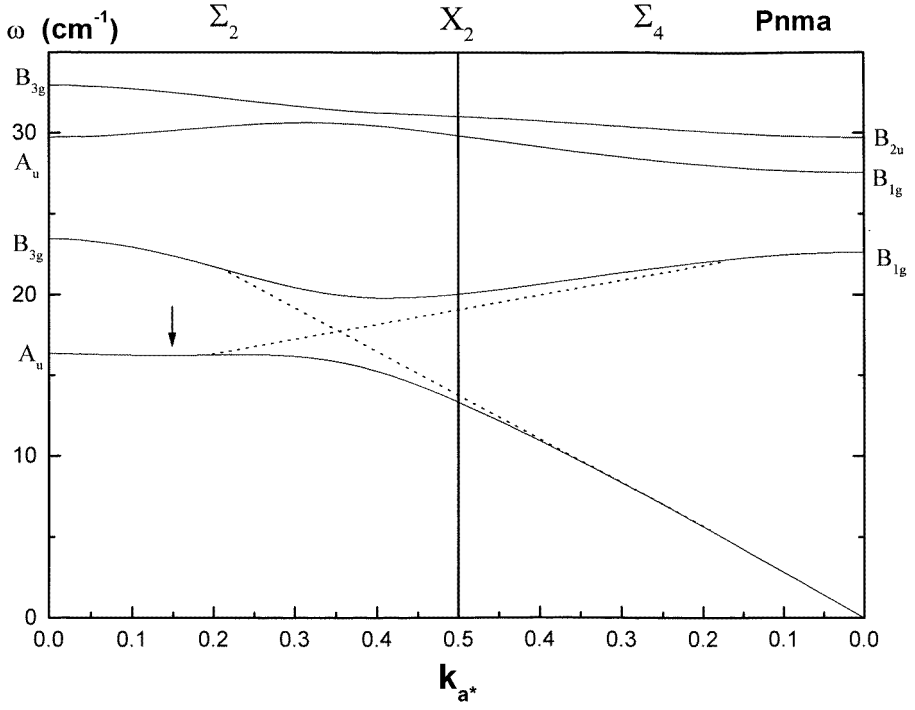

Figure 3. Low-frequency branches of Cs_2CdBr_4 in the *Pnma* phase along the $\boldsymbol{a}^*$-direction. The dashed lines indicate the possible anticrossing of phonon branches.

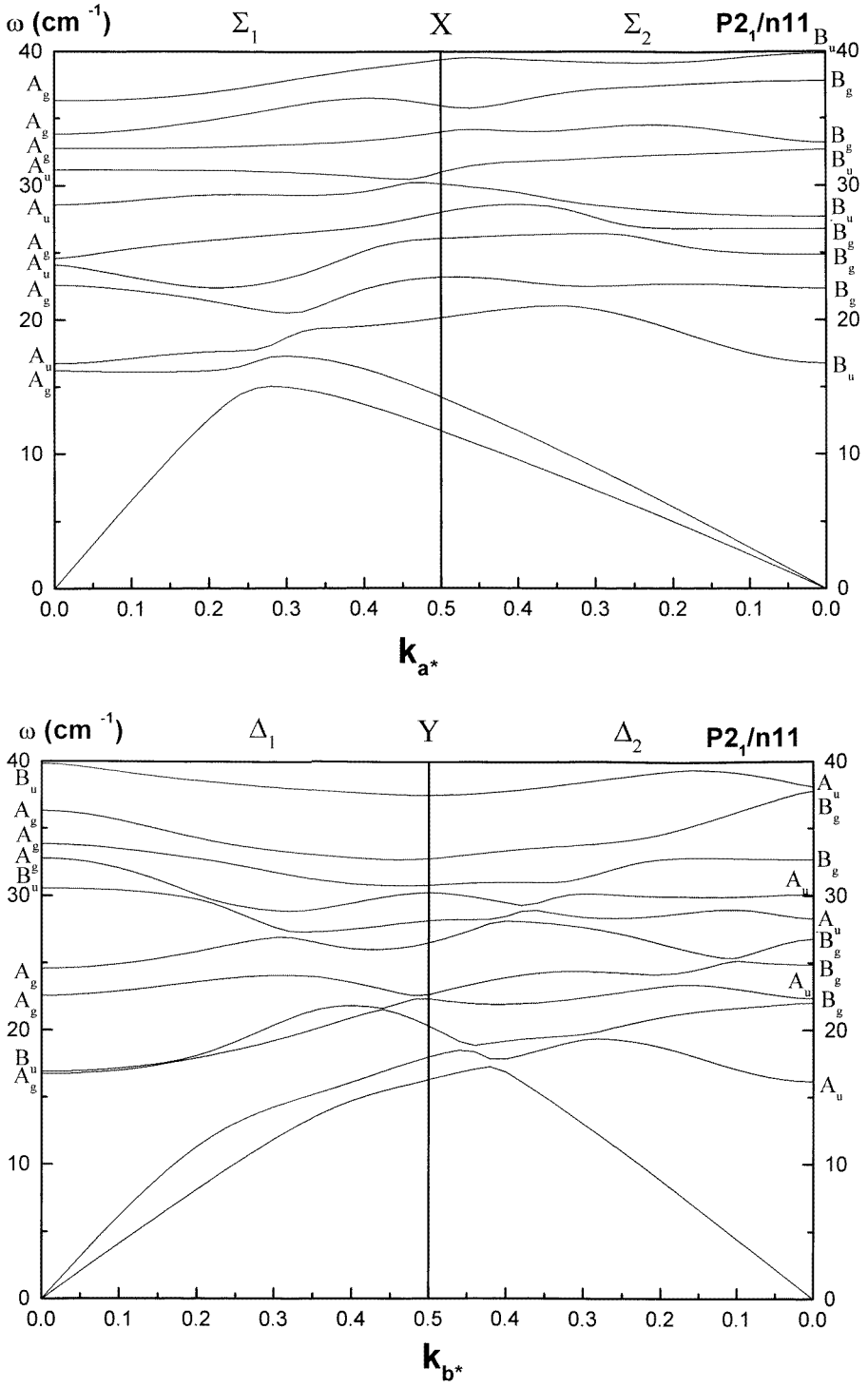

Figure 4. The low-frequency part of the phonon dispersion branches of the Cs_2CdBr_4 crystal in phase IV ($P2_1/n11$).

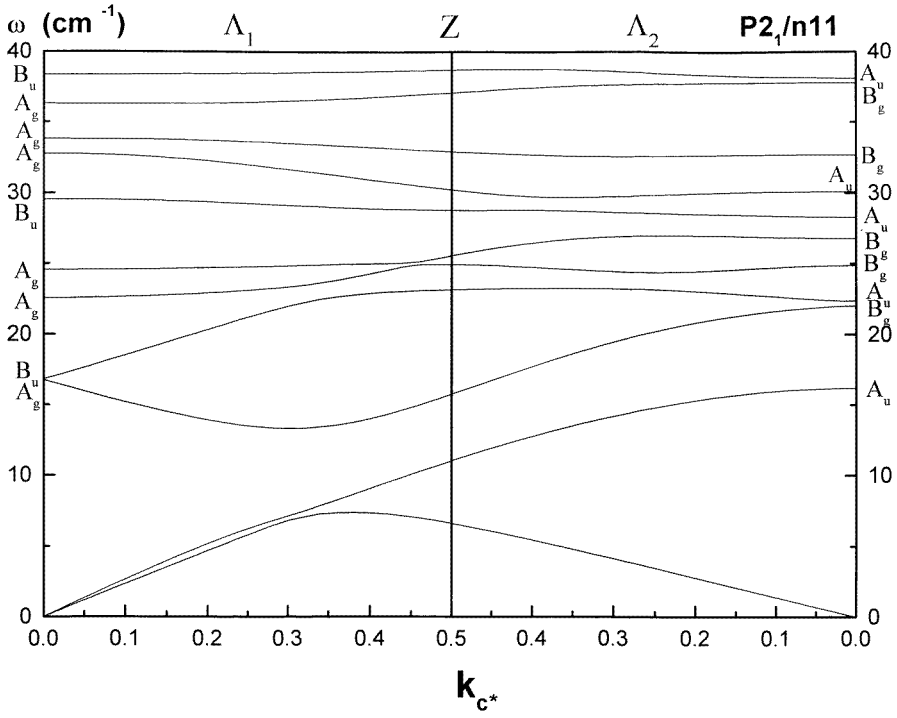

Figure 4. (Continued)

form $(\mathrm{d}S/\mathrm{d}x)R - S(\mathrm{d}R/\mathrm{d}x)$. At room temperature the calculated lower-frequency coupled Σ_2 phonon branch has a shallow minimum near $0.15\boldsymbol{a}^*$ (see figure 3) close to the observed value of the IC wave vector $\boldsymbol{k}_i$. Therefore it seems reasonable to assume that the normal–IC transition at $T_i = 252$ K is triggered by softening of this minimum. Due to the probable order–disorder nature of the transition, this softening might not be complete.

It is worth noting that the active representation which induces the direct zone-centre I–III transition is B_{3g}, whereas the lowest Σ_2 branch ends in A_u symmetry (figure 3). It is therefore probable that both the I–II and II–III transitions are induced by softening of the higher-frequency Σ_2 branch ending in B_{3g} symmetry. This branch for $\boldsymbol{k} \neq \boldsymbol{0}$ is bilinearly coupled with the lowest Σ_2 branch by the above-mentioned Lifshitz-like invariant, which may cause partial softening of the latter branch.

4.2. Phase IV ($P2_1/n11$)

The dispersion curves of Cs_2CdBr_4 in this phase were calculated at 195 K using atomic coordinates and the effective parameters presented in tables 1 and 4, respectively. The comparison of the calculated phonon frequencies at the point $k_{a^*} = 0.001$ with the experimental ones is shown in table 6. According to our simulation, the values of most of the phonon frequencies changed insignificantly with respect to those of the high-temperature phase I. Only the frequencies in the region 85–145 cm^{-1} which correspond to the strongly mixed external–internal vibrations for all of the symmetry types reveal appreciable lowering by about 8–10 cm^{-1}. The low-frequency part of phonon dispersion curves in phase IV is presented in figure 4. One can see from this figure that there is considerable anticrossing of phonon branches, implying substantial coupling among branches.

Table 6. Comparison of the calculated and experimental phonon frequencies (in cm^{-1}) near the Brillouin zone centre in the monoclinic phase (IV) at 195 K.

A_g		B_g		A_u		B_u	
Calculations	Raman [20]	Calculations	Raman [20]	Calculations	IR [1]	Calculations	IR [1]
16	16	22	21	Acoustic		Acoustic	
23	18	25		17		Acoustic	
25	29	27		24		17	19
33	32	33		29		28	22
34		38	38	31	34	33	31
36	39	45	46	38		40	38
42	42	49		46	45	43	48
45	48	52	54	52	52	47	53
53	58	55	62	67		61	61
68		69	69	69	70	69	68
69		73		73		71	
72	72	76		76		73	73
86	84	85	82	85	85	89	83
101		99		97	97	98	
124		124		120		121	
136		138		133		134	
138		140		140		138	
170	170	171	170	174		169	
177	187	178	180	178	181	177	
185	195	186	189	190	196	185	183
204	205	204	193	204	208	203	203

Concerning the IV $\rightarrow$ V transition, an underdamped soft mode was observed in Raman spectra of $B_g(xy, xz)$ symmetry near this transition [19, 22]. More recent Raman investigation [20] has shown that the soft mode is active only in phase V and vanishes in phase IV. That is why the authors of reference [20] have assumed that the unit cell multiplies at the IV–V phase transition. As seen from table 6, the lowest calculated mode frequency of B_g symmetry at 195 K has the value 22 cm^{-1} (the experimental value is 21 cm^{-1} [19]). Modes of other symmetries have even smaller frequencies at the Brillouin zone centre, namely 17 cm^{-1} (16 cm^{-1} [20], A_g), 16 cm^{-1} (A_u) and 17 cm^{-1} (19 cm^{-1} [1], B_u) (experimental values of the frequencies are indicated in parentheses). Taking into account the compatibility relations of irreducible representations along the main directions of the Brillouin zone (see table 2) and the phonon dispersion in phase IV (see figure 4), we can suppose that the phonon branches with the frequencies lower than that of the lowest B_g mode but of the same symmetry away from the Γ point (e.g. B_u along the $\boldsymbol{a}^*$-direction and A_u along the $\boldsymbol{b}^*$- and $\boldsymbol{c}^*$-directions) would lose their stability before the lowest B_g mode. However, from symmetry, the softening of A_u or B_u modes cannot lead to the $P\bar{1}$ space group for phase V, which was observed experimentally [13, 23]. Therefore, softening of the B_g mode at the Brillouin zone centre at the IV–V phase transition seems to be unlikely.

There is another possibility for realization of the $P\bar{1}$ space group in phase V, namely condensation of some phonon at the Brillouin zone boundary. The $P\bar{1}$ space group could be realized due to phonon softening at points A, Z and E (for the notation see [16]) or due to the softening of a doubly degenerate phonon mode which transforms according to the two-dimensional irreducible representation at points Y and C. All such transitions are connected with a multiplication of the unit cell. This could explain the observation of the soft mode in

Raman scattering [20] in phase V only. Additional experimental and theoretical investigations (e.g. simulation of temperature changes of phonon spectra in phase IV, like in reference [24]) are desirable in order to find unambiguously the soft mode and order parameter for the IV–V phase transition.

5. Conclusions

Investigation of the lattice stability conditions in the framework of the atomic model confirms the assumption proposed in reference [13] of inequivalent distribution of effective charges of (i) Cs1 and Cs2 ions and (ii) Br1, Br2 and Br3 ions in the Cs_2CdBr_4 crystal. The large difference between the Cs1 and Cs2 charge (0.53 and 1.02, respectively) in the $Pnma$ phase is reduced at 195 K due to the increase of the Cs1 charge (to 0.64).

The reasonable agreement between the calculated and experimental values of the phonon frequencies reveals the expediency of the Cs_2CdBr_4 lattice dynamics simulation using and interatomic potential which includes long-range Coulombic, short-range and covalent-bond interactions. The study of the phonon spectrum was complicated due to the mixed external–internal character of nearly all phonon modes.

Numerical lattice dynamics simulation demonstrates the substantial coupling of low-lying Σ_2 phonon branches at room temperature. It causes a shallow minimum near $\boldsymbol{k}_i \approx 0.15\boldsymbol{a}^*$ on the lowest Σ_2 optic branch, whose softening could explain the appearance of the IC structure. This result is in good agreement with the idea proposed in reference [22] that the IC phase in isomorphous Cs_2HgBr_4 is realized due to the presence of a Lifshitz-like invariant in the free-energy expansion.

From numerical simulations of the phonon dispersion branches and analysis of experimental data, it follows that softening of any B_g mode at the Brillouin zone centre in the $P2_1/n11$ phase IV is highly improbable. Instead, condensation of a phonon mode at the Brillouin zone boundary (e.g. at the points Y ($\boldsymbol{k} = (1/2)\boldsymbol{b}^*$), Z ($\boldsymbol{k} = (1/2)\boldsymbol{c}^*$) or C ($\boldsymbol{k} = (1/2)[\boldsymbol{b}^* + \boldsymbol{c}^*]$) is suggested, which could lead to the $P\bar{1}$ symmetry of phase V with the unit-cell multiplication. However, in order to understand properly the mechanism of the IV–V phase transition, as well as of the IC one, further experiments as well as lattice dynamics simulations of lattice instability conditions at phase transitions are necessary.

Acknowledgments

The authors would like to thank V Dvořák, P Kužel and J Hlinka for helpful discussions and a critical reading of the manuscript. The work was supported by the Czech Grant Agency (project No 202/98/1282), the Grant Agency of the Academy of Sciences of the Czech Republic (project No A1010828) and by the Ministry of Education of the Czech Republic (project Kontakt ME 100).

References

[1] Shchur Ya, Kamba S and Petzelt J 1999 *J. Phys.: Condens. Matter* **11** 3601
[2] Gervais F 1983 *Infrared and Millimeter Waves* vol 8, ed K J Button (New York: Academic) p 435
[3] Haque M S and Hardy J R 1980 *Phys. Rev.* B **21** 245
[4] Iizumi M, Axe J D, Shirane G and Shimoaka K 1977 *Phys. Rev.* B **15** 4392
[5] Etxebarria I, Perez-Mato J M and Criado A 1990 *Phys. Rev.* B **42** 8482
[6] Chaplot S L, Rao K R and Roy A P 1984 *Phys. Rev.* B **29** 4747
[7] Katkanant V, Lu H M and Hardy J R 1992 *Phys. Rev.* B **46** 5982
[8] Shchur Ya I, Kityk A V, Trach I B and Vlokh O G 1998 *Ukr. Fiz. Zh.* **43** 852

[9] Lu H M and Hardy J R 1990 *Phys. Rev.* B **42** 8339
[10] Lu H M and Hardy J R 1992 *Phys. Rev.* B **45** 7609
[11] Lu H M and Hardy J R 1992 *Phys. Rev.* B **46** 8582
[12] Altermatt D, Arend H, Niggli A and Petter W 1979 *Mater. Res. Bull.* **14** 1391
[13] Altermatt D, Arend H, Gramlich V, Niggli A and Petter W 1984 *Acta Crystallogr.* B **40** 347
[14] Nakamoto K 1978 *Infrared and Raman Spectra of Inorganic and Coordination Compounds* (New York: Wiley)
[15] Maradudin A A and Vosko S H 1968 *Rev. Mod. Phys.* **40** 1
[16] Bradley C J and Cracknell A P 1972 *The Mathematical Theory of Symmetry in Solids* (Oxford: Clarendon)
[17] Chaplot S L and Sahni V C 1979 *Phys. Status Solidi* a **96** 575
[18] Boyer L L and Hardy J R 1973 *Phys. Rev.* B **7** 2886
[19] Rodriguez V, Couzi M, Gomez-Cuevas A and Chaminade J P 1991 *Phase Transitions* **31** 75
[20] Torgashev I, Yuzyuk Yu I, Burmistrova L A, Smutny F and Vanek P 1993 *J. Phys.: Condens. Matter* **5** 5761
[21] Chaplot S L 1978 *Bhabha Atomic Research Centre, Bombay, Report* BARC N 972
[22] Plesko S, Dvořák V, Kind R and Treindl A 1981 *Ferroelectrics* **36** 331
[23] Maeda M, Honda A and Yamada N 1983 *J. Phys. Soc. Japan* **52** 3219
[24] Kityk A V, Shchur Ya I, Zadorozhna A V, Trach I B, Girnyk I S, Martynyuk-Lototska I Yu and Vlokh O G 1998 *Phys. Rev.* B **58** 2505